On the location of X-ray peaks and dominant galaxies in clusters

Davide Lazzati[1,2] **and Guido Chincarini**[1,2]

[1] Osservatorio Astronomico di Brera, via E. Bianchi 46, I-23807 Merate (Lc), Italy
[2] Università degli Studi di Milano, via Celoria 16, I-20133 Milano, Italy

Abstract. We analyze the structure of the X-ray emission of a sample of 22 Abell clusters of galaxies with a cD in their centre, observed with the ROSAT PSPC. Utilizing the multi-scale power of the Wavelet Transform we detect significant ($\sim 50\,h^{-1}$ kpc) offsets between the large scale centroid and the peak of X-ray emission. Despite the uncertainties on the satellite pointing, the X-ray to optical correlation indicates a likely association between the X-ray peak and the dominant galaxy. We develop a model in which the offset is produced by small amplitude oscillations of the cD galaxy around the bottom of the cluster potential well and successfully compare it to the observed distribution of offsets. Within this scenario the offsets are not due to dynamic instabilities and the number of structured clusters is greatly reduced.

Key words: galaxies: clusters: general – galaxies: elliptical and lenticular, cD – X-rays: galaxies

1. Introduction

It is well known that the presence of a dominant galaxy (cD) in the core of a galaxy cluster is a sign of dynamical evolution, being highly correlated with a smooth spatial distribution and a low spiral fraction of member galaxies (Sarazin 1988).

In a large fraction of clusters with cDs, the X-ray peak is offset with respect to the centroid of large scale emission (Mohr et al. 1993, 1995). Whether these offsets are caused by substructure, due to the infall of smaller groups of galaxies, or not, is still an open issue. Indeed, the fraction of clusters with substructure is strongly linked to the density parameter Ω_0 (Richstone et al. 1992; Nakamura et al. 1995) and any spurious substructure would confuse the potential link between observed cluster morphologies and that expected theoretically.

In a sample of 22 X-ray images of Abell clusters with cD galaxies in their centre (see Sect. 2 for the description of the sample), we find that the peak of the X-ray emission is always located about the position of the dominant galaxy and is offset from the large scale centroid. In this work we propose an alternative to infall or Intra Cluster Medium (hereafter ICM) instability models to explain the presence of these offsets since: a)

these phenomena are unexpected in clusters which have the appearance of being relaxed systems (cooling flows and dominant galaxies); b) infall would disrupt the cooling flow and produce substructure with higher frequency in the outskirts of clusters rather than in their centre, and c) the asymmetries observed in the ICM would have to be independent of the cD position.

In our model a strong and compact X-ray source is associated with the dominant galaxy which in turn moves about the bottom of the cluster potential well with harmonic oscillations, producing the observed offset. Whether this compact source is a cooling flow or an active nucleus is not essential and will be discussed in the last section. Such a model provides a natural explanation of the facts summarized above without invoking any dynamical instability. As a consequence, the fraction of structured clusters is reduced from more than 70% (Davis 1994) down to about 30%.

The role of cD galaxies and their motion relative to the bottom of the cluster potential well is still a matter of debate. Optical observations, which should be best suited for such an analysis, suffer from low number statistics in the cluster and the results are somewhat contradictory. Studies on individual clusters (Hill et al. 1992; Sharples et al. 1988; Oegerle & Hill 1992) find significant peculiar radial motions of the cD with respect to the mean recession velocity, and in sample of 25 cD clusters Zabludoff et al. (1990) find that "a substantial fraction of the cD galaxies have velocities significantly different from the mean of their parent clusters", a result confirmed by Malumuth et al. (1992). However it is not completely clear whether the presence of substructure in the velocity field could alter this result (Oegerle & Hill 1994; Bird 1994).

Numerical simulations of cluster evolution (Richstone & Malumuth 1983; Malumuth & Richstone 1984) predict that cD galaxies are created and spend their existence near the centre of clusters and move slowly around them. Moreover, the actual motion of the dominant galaxy and the related displacement from the bottom of the potential well are also an important clue to understand the formation scenario of dominant galaxies (see Oegerle & Hill 1994 and references therein).

By assuming that cD galaxies move about the centre of mass of their parent clusters we can derive an equation of motion and estimate a normalized oscillation amplitude which is independent from the parameters of the individual clusters. We can then

---

Send offprint requests to: Davide Lazzati

Table 1. Properties of the cluster sample and of the respective PSPC observations.

Abell number	z	ROR	Exposure (s)	Photons[1]	$\dot{M}$[2]
85	0.0556	800250	10238	16836	108.0
133	0.0566	800319	19404	9358	110.0
262	0.0161	800254	8686	9559.	9.4
400	0.0232	800226	23611	11856	0.0
478	0.0880	800193	21969	12877	736.0
496	0.0320	800024	8857	13215	134.0
539	0.0205	800255	9646	7711	2.1
1060	0.0114	800200	15764	36310	8.0
1651	0.0825	800353	7429	6400	0.0
1795	0.0616	800105	36273	43724	321.0
1991	0.0586	800518	21261	6157	37.0
2029	0.0767	800249	12542	18989	431.0
2052	0.0350	800275	6211	7813	94.0
2063	0.0337	800184	9763	9794	35.0
2107	0.0421	800509	8274	5508	7.1
2142	0.0899	800551	6090	8881	369.0
2589	0.0421	800526	7289	6339	-
2657	0.0414	800320	18904	12487	44.0
3562	0.0490	800237	20199	13503	0.0
3921	0.0936	800378	11997	7263	-
4038	0.0292	800354	3353[3]	4845	-
4059	0.0488	800175	5439	5876	-

[1] Approximate number of photons (background subtracted) used in the large scale centroid determination
[2] Cooling flow mass rate in solar masses per year (from Fabian 1994; White et al. 1997; Allen & Fabian 1998). A long dash indicates clusters for which no data have been found.
[3] This exposure is lower than the 5 ks limit set for the sample, but a sufficiently accurate measurement of the centroid has been possible.

compare the expected distribution of the normalized amplitudes to the measurements from the set of 22 X-ray images of moderate redshift Abell clusters.

This paper is organized as follows: Sect. 2 describes the data and the reduction procedures, Sects. 3 and 4 describe respectively the small and large scale analysis performed on the images, while Sect. 5 briefly summarize the measured offset properties. The possible identification of the cD galaxy with the emission peak is discussed in Sect. 6; Sect. 7 describes the physical oscillatory model and the results are summarized and discussed in Sect. 8.

2. The data: selection criteria and preliminary reduction

To detect a small but significant offset between the peak and the large scale emission of clusters we need a precise determination of both these positions.

The uncertainty on the determination of the position of a source characterized by a profile with a width σ (irrespective of whether it is intrinsic or due to the instrument resolution) and a number N of counts is given by:

$$\Delta(x) \simeq \frac{\sigma}{\sqrt{N}} \qquad (1)$$

which follows from the standard error propagation rules. The exact equality holds for a Gaussian spatial distribution of photon counts.

Hence, for a point-like source, the best instrument to measure the position maximizes the value of the ratio $\sqrt{\varepsilon}/\sigma_{(d)}$, where ε is the detector efficiency and $\sigma_{(d)}$ its intrinsic resolution. However, when the angular dimension of the source is intrinsic - as is the case for the ICM X-ray emission - the width of the photon distribution is fixed and only a higher value of ε can increase the position accuracy.

Given the above discussion, the cluster observations have been extracted from the ROSAT/PSPC archive maintained by the ROSAT group at the *Max Plank Institut für Extraterrestrische Physik* in Garching (D). We have selected a set of observations pointed on Abell clusters (Abell et al. 1989) with cD galaxy in their centre and a known value of the radial velocity dispersion. Other constraints were an exposure time greater than 5 ks and an angular dimension an order of magnitude greater than the resolution in the centre of the PSPC field ($\sim 40''$ FWHM).

As of March 1995, we found 22 clusters with ROSAT/PSPC pointed observations that met the above requirements, listed in Table 1 along with their main properties. All these observations have $N \gtrsim 5 \times 10^3$ counts in the cluster large scale emission. With a typical width of $3r_c \simeq 7.5'$ for the clusters as a whole, Eq. 1 gives an accuracy of $6''$ in the determination of the centroid, where r_c is the core radius of the modified King function that better fits the cluster profile. We have used $3r_c$ as cluster width to properly take into account the wider wings of the King function with respect to the Gaussian distribution.
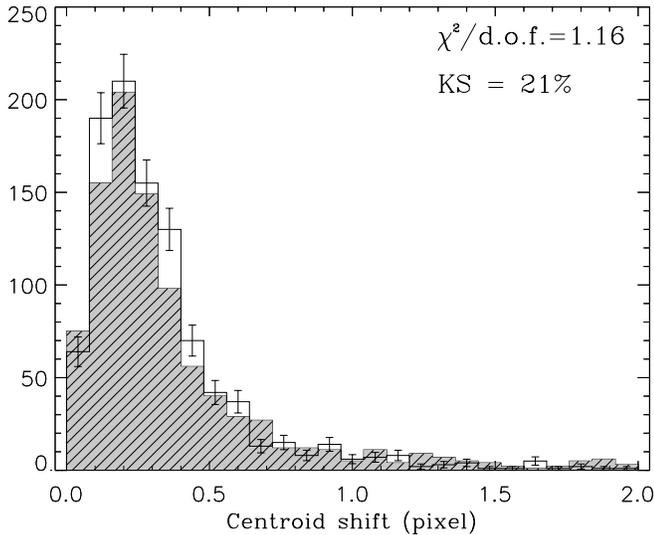
Fig. 1. Influence of the compact source on the centroid determination. Histogram of the distance between input and output centroids are plotted for the simulations with (shaded region) and without (solid line) the offset compact source. The distributions are consistent with being two realizations of the same parent. See the text for the statistical test results.

The central compact source - which in our model is responsible for the emission peak - has a mean number of $\gtrsim 1000$ photons and a width comparable to the PSPC central resolution of $\sim 25''$ ($1\,\sigma$). Eq. 1 gives an accuracy $\Delta(x) \lesssim 1''$.

The precision on the determination of the peak position could be increased using a detector with higher resolution as the ROSAT HRI. However, the efficiency of this instrument is lower than that of the PSPC and hence the accuracy of centroid measurement would be decreased. Note that to avoid any influence of the boresight errors (see Sect. 6) it is crucial that both the centroid and the peak positions are measured on the same image.

The image reduction has been performed with the complete treatment included in the ESAS software (Snowden 1995) which takes into account all the properties of the PSPC instrument and of the particular observation (solar contamination and short and long term enhancements of the cosmic background, see Snowden et al. 1994). This is because instrumental effects such as vignetting, detector efficiency, particle background etc. conspire to build a large scale structure in the images. This structure, if uncorrected, has its centre coincident with the image centre and could efficiently mimic an offset with the peak of the true emission.

We have tested the complete reduction process searching for large scale residuals in PSPC point-like source images. We found no evidence for such an effect in the analysis of a set of 20 images.

Due to different distance and intrinsic cluster dimensions, we have implemented specific ESAS routines in order to obtain images with dynamic pixel size. The final images (512×512 pixels each) have a pixel size (1 pixel $= 4 \div 10''$) chosen to
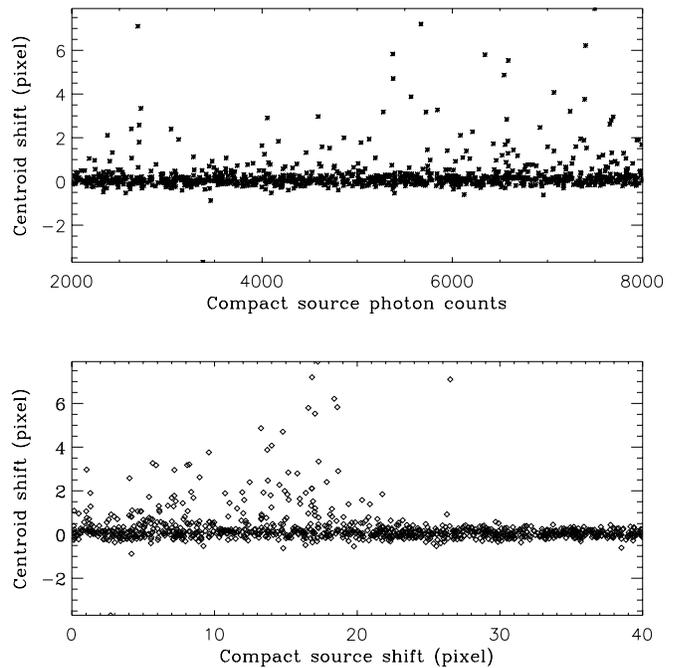

Fig. 2. Influence of the compact source on the centroid determination. Measured x-axis errors on the centroid position versus the photon counts in the offset peak are plotted in the upper panel. The vast majority of measurement have a dispersion lower than one pixel, but a limited number of centroid measurement are shifted towards the compact source (positive values in both panels). No clear dependence of this shift on the power of the compact source is seen. The lower panel show the same position errors in the measured centroid versus the offset of the input compact source. In this case a trend with the compact source centroid is visible. The trend disappears for offsets larger than 20 pixels, almost the size of the core radius of the large scale emission. Note that in both cases the errors in the centroid measurements tend to mask the effect of displacement between the centroid and the emission peak.

maintain a fixed (small) ratio between the whole image width and the cluster angular dimensions.

To fully explore any possible bias due to the reduction process we could simulate a set of cluster images with instrumental effects included and than compare the cluster parameters obtained after the reduction with those input in the simulations. However, this procedure is extremely time consuming and any unknown instrumental effect would remain undetected.

3. Small scale analysis

Once a cleaned count-rate image has been obtained, a wavelet transform algorithm is applied to search for small scale structures embedded in the cluster emission. We use the algorithm expressly designed to detect and characterize small structures overlaid on strongly varying backgrounds presented and discussed in Lazzati et al. (1998).

The wavelet transform algorithm spans scales from half the PSF on-axis up to about twice the PSF at the edges of the image, with a spacing of a factor of two between adjacent scales. This
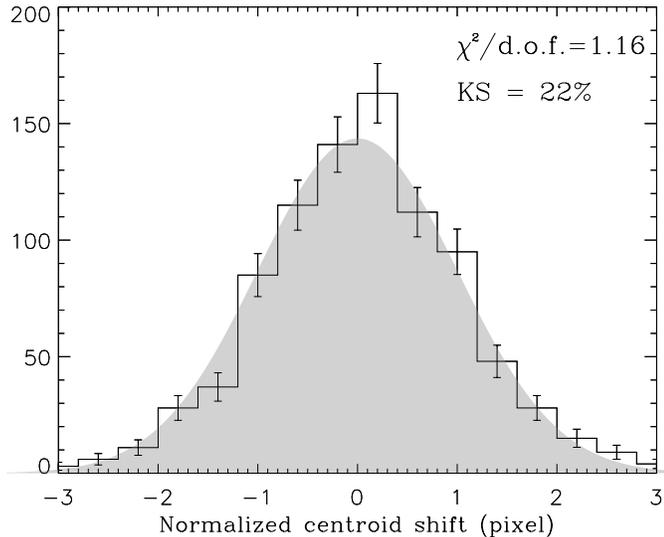
Fig. 3. Histogram of the measured errors in recovering the large scale centroid normalized to the uncertainties derived from the covariance matrix. The distribution appears consistent with a Gaussian distribution with a normal standard deviation (shaded area).

Table 2. Properties of the clusters simulated to test the centroid determination procedure. All distributions are flat except ellipticity and β which have Gaussian probability functions.

	LS[1]	e [2]	β	SS[3]	$\Delta(x)$[4]	$\Delta(y)$[4]
average	15000	0.8	0.76	5000	40	40
width	10000	0.07	0.25	3000	20	20

[1] Number of counts in the large scale cluster emission.
[2] Ellipticity defined as the ratio between the minor and major axis.
[3] Number of photon counts in the offset compact source.
[4] Offset of the compact source in the x and y directions in pixels with respect to the large scale centroid.

procedure guesses the position of the emission peak and selects a set of "point sources" to be masked in the subsequent large scale analysis (see Sect. 4).

The emission peak position is then refined fitting a bidimensional Gaussian source model to the image in the wavelet space. Since the covariance matrix highly underestimates uncertainties in correlated data sets, the uncertainties on the peak position are estimated in χ^2 space. A χ^2 shift of 4.61 is used in order to obtain 90% confidence intervals for two independent degrees of freedom (position in both directions). Again, this procedure is not strictly correct in the presence of correlations between data points. Rosati (1995) performed several tests to see if any systematic error could arise, confirming the reliability of this procedure.

Note, however, that the uncertainties on the peak position are in most cases negligible with respect to those in the large scale centroid, which contribute the largest uncertainties to the offset measurement.

4. Large scale analysis

Great care must be used in the determination of the centroid position since the offset we are looking for is considerably smaller than the whole cluster emission. To obtain the best position for the centroid of the large scale emission, we fit the cluster emission with an elliptical β model:

$$I_X(r, \vartheta) \propto \left[1 + \left(\frac{r}{r_c(\vartheta)}\right)^2\right]^{-3\beta + \frac{1}{2}}, \qquad (2)$$

where $r_c(\vartheta)$ is the azimuth dependent core-radius. The central part, affected by the presence of the compact source, was excluded from the fit as well as all the point-like sources detected

in projection over the cluster emission. A bidimensional Gaussian smoothing of the image was necessary to obtain a more accurate estimate of the statistical distribution of points.

To test the reliability of this procedure we have simulated a set of 1000 clusters with properties that span the range of our sample which are summarized in Table 2. The core radius of the clusters has been fixed to 20 pixels[1] while all the remaining shape parameters have been randomly picked up each time from the distributions described in Table 2. To fully reproduce the experimental images, an offset Gaussian source ($FWHM = 12$ pixels, slightly bigger than a point-like source) with a lower number of counts has been added in the cluster centre and then the centroid has been measured with the procedure described above. Analogous simulations have been performed without the compact offset Gaussian source for comparison.

Figs. 1, 2 and 3 show the result of these simulations. To see whether the presence of the compact offset source could produce a systematic error in the centroid determination we have compared the position errors measured from simulations with and without the compact source. Fig. 1 shows the histogram of the distance between input and output centroid positions in both cases. The similarity between the two distributions is confirmed by the Kolmogorov-Smirnov test, which gives a $\sim 21\%$ probability of them both deriving from the same parent distribution. Moreover, by fitting the difference of the two distributions with a zero constant we have obtained a reduced χ^2 value of 1.16. The absolute values of the distance between the true and the measured centroid are around a quarter of a pixel, which, given the resolution of our images, translates in an uncertainty in the range $1'' - 2.5''$, a value suitable for our requirements (see Sect. 2).

When the offset Gaussian source is present in simulations, the distribution of the shift between input and output centroids has a tail that is considerably higher than what expected in a Gaussian distribution (the positive values in Fig. 2). This effect increases with the shift between the centroid and the peak position (lower panel of Fig. 2) up to a sharp cutoff when the shift becomes larger then the core radius. We can confidently ignore this effect since it tends to reduce the measured offset and not to create it spuriously.

---

[1] This is not a restriction of simulations since the image size has been chosen to preserve a fixed dimension of the cluster in pixels.
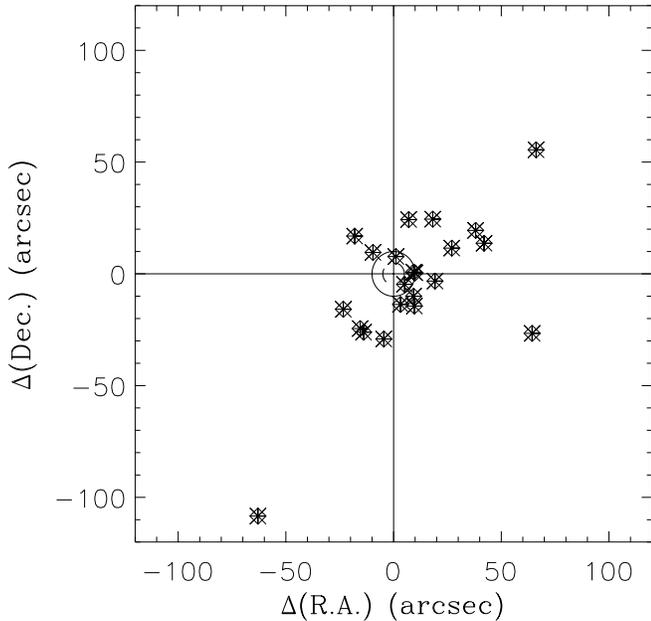
Fig. 4. Positions of the large scale centroids with respect to the emission peak. The peak is located in the origin of coordinates and shifts in right ascension and declination are given in arcseconds. The dashed circle encloses the $5''$ confidence region (see text) for the centroid position while dotted circle marks the $10''$ region.

Finally, we have tested the reliability of the uncertainties extracted from the covariance matrix. If these are correct, the errors measured in the simulations divided by those estimated in the fitting procedure should be distributed as a Gaussian with normal standard deviation. As shown in Fig. 3 this is what actually happens. The observed distribution is consistent with a Gaussian parent at the 22% level with a Kolmogorov-Smirnov test. A fit with a Gaussian gives a reduced χ^2 of 1.17.

5. Offsets

Applying the procedure described and tested above to the X-ray images we are able to measure the offsets of the cluster sample along with their uncertainties. The values of centroid position errors estimated in the fitting procedure were always $\lesssim 5''$ but, to be conservative, we adopt this value for the whole set of clusters.

The results are shown in Fig. 4 where the emission peak lie at the center of coordinates and the symbols mark the position of the centroid. The inner circle radius is $5''$ ($1\,\sigma$), while the outer is $10''$. Only 4 measurements over 22 are in agreement with the absence of any offset at the $2\,\sigma$ level. Fig. 5 shows the offsets distribution in physical units; the actual displacements are always lower than $60\ h^{-1}$ kiloparsec, a value smaller than the typical core radius of the ICM distribution.

A final test to see if the characteristics of the detector play a role in the offset measure can be finally performed on experimental data. If the measured offsets were produced by some unknown instrumental effect, we would expect to find a correlation between the redshift of the cluster and the offset measured
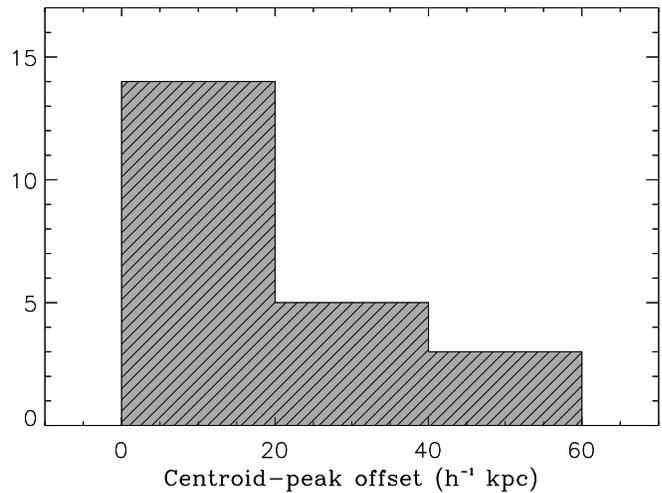

Fig. 5. Distribution of the measured offsets in physical units.

in physical units (kiloparsec). The linear Pearson correlation coefficient r between the two dataset is $r = 0.25$. The probability that two uncorrelated 22 elements datasets give a value of $r > 0.25$ is $P = 40\%$.

6. X-ray cD counterparts

Once the presence of offsets has been firmly established, we can try to correlate both X-ray positions with the optical position of the dominant cluster galaxy.

Unfortunately, the comparison between optical and X-ray positions suffer the boresight problem, i.e. an absolute error in the satellite pointing which turns in a systematic shift between sources positions and respective optical counterparts. This error can be corrected when at least 2 bright X-ray sources in a single image can be correlated with bright optical objects (e.g. Guide Star Catalog objects). If uncorrected, the boresight error is estimated to have a Gaussian distribution with standard deviation of $\sim 10''$ both in right ascension and declination (see the *ROSATSRC* catalog, Zimmermann 1994).

In the A478 image, after the application of a $12''$ boresight correction, the X-ray peak position is only $3''$ away from the cD optical position.

No X-ray source correlated to a Guide Star Catalog object was found in the remaining 21 images and, given the rather large pointing error, it has not been possible to establish a firm identification of the cD galaxy as the object that produces the offset peak in the large scale X-ray emission of the ICM. However, we can state that within these uncertainties the position of the X-ray peak coincides with the galaxy. In Fig. 6 we show the distribution of X-ray peak positions around the cD which lies in the origin of the coordinates. The circles represent 1σ and 2σ confidence regions. As expected, 40% (9 over 22) of the X-ray peaks lie inside the 1σ circle. The distribution of the right ascension residuals in Fig. 6 appears biased towards negative shifts. The tests performed on the analysis procedure described in Sect. 4 shows that no bias is present in the X-ray positions and the ac-
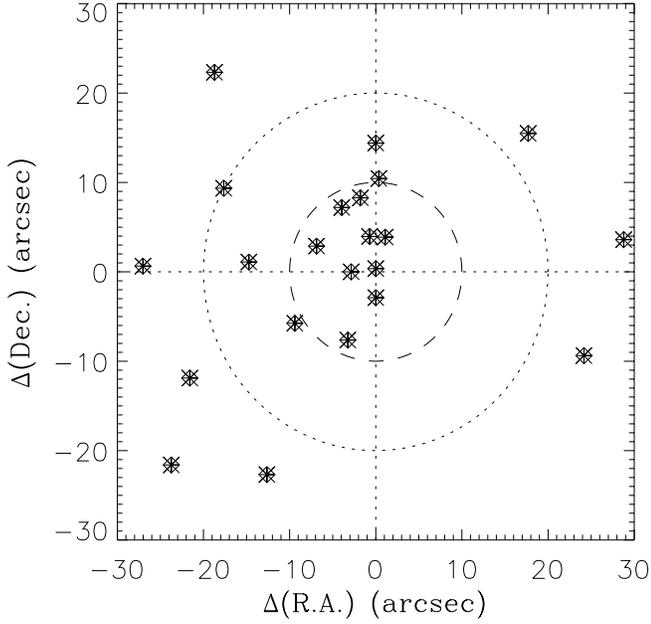
Fig. 6. Relative positions of the X-ray peaks with respect to the cD galaxy. The cD is located in the origin of coordinates and shifts in right ascension and declination are given in arcseconds. The dashed circle encloses the 1σ confidence region for the boresight error while dotted circle marks the 2σ region.

curacy of Guide Star Catalogue is fully adequate; moreover, the absence of the effect in the declination shifts indicates that the the analysis procedure is unbiased. The binomial probability of obtaining such a skewed dataset from a symmetric distribution is $P = 3.2\%$.

If the difference between the peak and X-ray positions were not due to instrumental effects we would expect a correlation between angular offset and redshift. The correlation coefficient between these two datasets is $r = -0.11$.

The possible identification of the cD galaxy with the peak of the cluster emission has been discussed in several papers. Allen et al. (1995) find a coincidence of the two positions in clusters that host a massive cooling flow in their centre, but do not find evidence of centroid shift in their sample; more often, a coincidence between the orientation of the cD isophotes with the ICM emission major axis is found (Sarazin & McNamara 1997; Huang & Sarazin 1998).

Given the identification, we can discuss a model that predicts the amount of separation between the X-ray peak and the bottom of the potential well of the ICM, marked by the centroid of large scale emission.

7. The oscillatory model

An implication of the above discussion is that the cD galaxy is not located in the bottom of the potential well and hence cannot be at rest but must oscillate around the equilibrium position. This wobbling produces the observed offset.

With a small set of reasonable assumptions and/or approximations on cluster structure, we can obtain the equation of

motion of the cD in the bottom of the potential well. First, since dominant galaxies are found well inside the core radius of clusters (Sect. 5), we assume that the mass inside the area of oscillation is uniformly distributed.

In clusters that host a massive cooling flow in their centres great deviations from uniformity could be present in the baryon fraction, however they will have a small effect on the total mass distribution and hence do not invalidate our model. We have therefore:

$$
\begin{aligned}
m_G \ddot{x} &= F = -G \frac{M_{int}\, m_G}{x^2} \\
&= -\frac{4}{3}\pi\, G\, \rho_{tot}\, m_G\, x
\end{aligned}
\tag{3}
$$

where m_G is the mass of the galaxy, M_{int} the mass contained in a sphere of radius equal to the position of the cD and ρ_{tot} the total mean mass density in the central part of the cluster. Solving Eq. 3 we obtain:

$$
x(t) = B\,\cos(\omega t + \varphi)
\tag{4}
$$

where:

$$
\omega = \sqrt{\frac{4}{3}\pi\, G\, \rho_{tot}}
\tag{5}
$$

The actual values of B_j and φ_j for the *j-th* cD galaxy are linked to initial speed and position. Since we are concerned with quantities averaged on an ensemble of clusters, we expect the values of the phases φ to be erased. The value of B can be obtained by assuming the *rms* speed of the galaxy proportional to the radial velocity dispersion of the whole cluster. This seems to be a reasonable assumption in view of the fact that the kinematic of the cD, whatever it is, must be related to the cluster potential well.

Putting this relation in our model we have:

$$
\begin{aligned}
\sigma_v^2 &= <v^2> - <v>^2 = <v^2> \\
&= B^2\,\omega^2 <\sin^2(\omega t)>
\end{aligned}
\tag{6}
$$

from which:

$$
B^2 = \frac{2\sigma_v^2}{\omega^2} = \frac{3}{2}\,\frac{\sigma_v^2}{\pi\, G\, \rho_{tot}}
\tag{7}
$$

We can hence define an adimensional oscillation amplitude Γ normalized to the individual cluster properties that should be distributed as an ensemble of identical harmonic oscillators with the same amplitude but with random phases and seen from random orientations.

$$
\Gamma = \sqrt{\frac{2\pi G}{3}}\,\frac{c z d_\vartheta}{H_0}\,\frac{\rho_{tot}^{1/2}}{\sigma_v}
\tag{8}
$$

$$
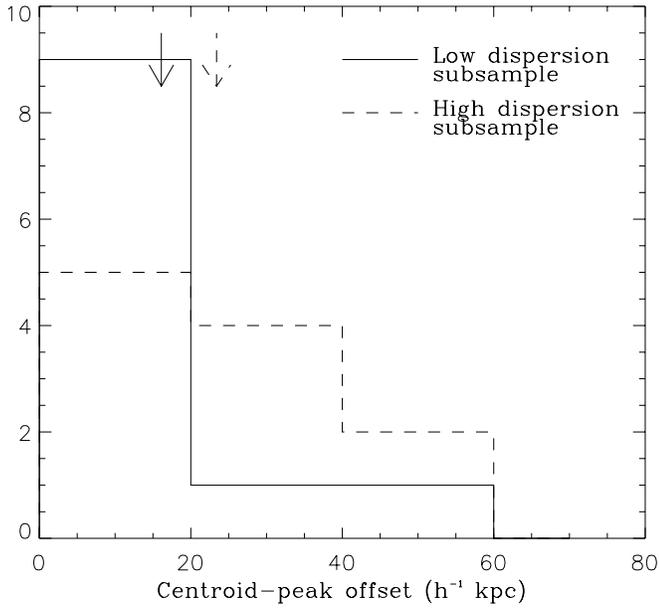p(\Gamma) \propto \int_\Gamma^L \frac{dl}{\sqrt{(l^2 - \Gamma^2)(L^2 - l^2)}}
\tag{9}
$$

Fig. 7. Dependence of the physical offset from the radial velocity dispersion. The offset histogram of the high dispersion subsample ($< \sigma_v > = 888 km/s$, dashed line and arrow) is significantly larger than that of the low dispersion ($< \sigma_v > = 597 km/s$, solid line and arrow) one. The arrows mark the mean value of the two distributions.
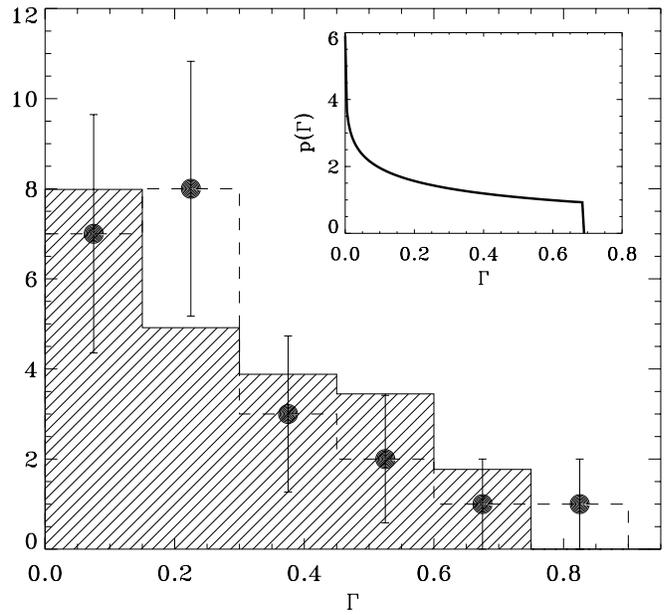

Fig. 8. Histogram of the values of the Γ parameter, as described in the text. The shaded area represents the expected distribution binned with the same width of data. A Kolmogorov-Smirnov test gives a $\sim 75\%$ probability of success. The insert shows the theoretical distribution (Eq. 9) before the binning process. Poissonian errors are drawn on experimental points.

where L is the largest oscillation amplitude allowed.

To test the likelihood of the assumption that the cD oscillation velocity is linked to the whole cluster velocity dispersion, made in Eq. 6, we have divided the sample in two subsamples based on their radial velocity dispersion. We expect the average offset to be proportional to the average velocity dispersion in the two subsamples. As is shown in Fig. 7, denoting with $_h$ and $_l$ respectively the high and low velocity dispersion subsamples we have:

$$< \sigma_v >_h = 888\,km/s \qquad < \Delta >_h = 23.4\,h^{-1}kpc$$
$$< \sigma_v >_l = 597\,km/s \qquad < \Delta >_l = 16.1\,h^{-1}kpc$$

from which:

$$\frac{< \sigma_v >_h}{< \Delta >_h} = 37.9 \quad \frac{< \sigma_v >_l}{< \Delta >_l} = 37.1 \qquad (10)$$

The major problem in the application of Eq. 8 is the determination of the central mean mass density. In fact, the X-ray emission of the ICM gives a direct information of the baryon density while what we need is an estimate of the total mean density in the cluster centres.

A crude estimate of the mean central density can be inferred applying the virial theorem with the measured cluster parameters σ_v and r_c:

$$\sigma_v^2 \simeq G\frac{M}{R} \quad \Rightarrow \quad \rho_{tot} \sim \frac{1}{G}\frac{\sigma_v^2}{R^2} \sim \frac{1}{G}\frac{\sigma_v^2}{r_c^2} \qquad (11)$$

Inserting this density in Eq. 8 we obtain:

$$\Gamma = \sqrt{\frac{2\pi}{3}}\frac{czd_\vartheta}{H_0}\frac{1}{r_c} = \sqrt{\frac{2\pi}{3}}\frac{d_\vartheta}{r_{c\,\vartheta}} \qquad (12)$$

where $r_{c\,\vartheta}$ is the apparent angular core radius.

A further problem that affect the comparison between the harmonic model and the observations is the intrinsic difficulty in measuring the core radius of clusters that host a cooling flow in their centre. This measurement is made highly inaccurate by the need of masking the central region of the cluster to get rid of the modification on the cluster central surface brightness due to the emission of the cool and dense inflowing gas (see, e.g. Allen & Fabian 1997). To see which uncertainty this problem could contribute to the final parameter Γ we have tested the change of the fitted value of the core-radius increasing the radius of the masked central region in the image of A1795. When the masked region is smaller than the PSF FWHM, the core radius is highly underestimated. If the mask radius is bigger than twice the PSF FWHM - any influence of the central compact source being completely erased - the core radius changes by a factor of 30% increasing the mask radius up to 5 times the above value. This uncertainty propagates with unchanged percentage in the determination of the value of Γ. Given the smooth shape of the probability distribution (Eq. 9) we expect that these uncertainties will affect only the high amplitude sharp cutoff and the low amplitude cusp of the function, leaving the overall shape unmodified (see the insert in Fig. 8).

Fig. 8 shows the distribution of the measured Γ in our cluster sample, compared with the theoretical distribution obtained re-

binning Eq. 9 (shaded area). The best value for the largest amplitude $L = 0.69$ has been obtained maximizing the Kolmogorov-Smirnov probability that the measured distribution is drawn from that theoretically derived. The maximum probability is $P_{K-S} \simeq 73\%$. Fig. 8 may suggest a slightly bigger value for the maximum amplitude L, however this would require a higher number of small offset clusters. This discrepancy can be ascribed to the crudeness of the model and, in particular, the introduction of circular (or even elliptical) cD orbits would erase the cusp of the distribution in the lowest offset region. Such a refinement of the model would however require a larger dataset to allow any quantitative comparison.

8. Conclusions and discussion

We have analyzed the structure of the X-ray emission of a set of 22 Abell cD clusters. We find evidence for a displacement between the centroid of the large scales and the peak of the emission, the latter being coincident with the dominant galaxy position.

The presence of centroid shifts in clusters with cD galaxies and cooling flows is problematic since such offsets are expected to be due to subcluster mergers, phenomena that would disrupt cooling flows (Meiksin 1988; Friaca 1993).

We have shown that, identifying the peak with the cD galaxy, an harmonic oscillator model for its motion in the cluster potential well is in agreement with present observations and with the predictions of the numerical simulations (Malumuth & Richstone 1984). It follows that offset peaks in X-ray images are produced by this oscillation and should not be thought as signs of dynamical instability and/or substructure.

From this interpretation, it follows that the compact emission in the centre (or near the centre) of clusters can be produced in principle inside the central galaxy or by a fraction of the ICM strongly linked to the galaxy itself. The first hypothesis can be easily discarded since observations of cluster central regions with high resolution instruments show that the compact source has a small but non-zero extension and hence cannot be due to an active nucleus (see, e.g., Grebenev et al. 1995, Pierre & Starck 1998). In the second scenario the cool and dense gas of the cooling flow could be responsible for the peaked emission seen in X-ray images and the offset would be caused by the motion of the cD galaxy. In this case the cooling flow - or at least its inner part - would have to follow the cD galaxy in its motion. Whether this is possible or such a motion would disrupt the frail flow stability has to be investigated in more detail. From the observational point of view, Pierre & Starck (1998) have analyzed a sample of high resolution images of clusters, finding that in the inner cores of massive cooling flow clusters the X-ray emission shows peculiar features and strong isophotal twisting (see their Fig. 6).

As a further consequence of this interpretation, the fraction of structured clusters is greatly reduced. In fact, in his analysis of a flux limited sample of X-ray clusters, Davis (1994) found a residual emission near the centre of clusters (but not coincident with them) after subtraction of the extended component with the elliptic isophotal fitting technique. The interpretation of this feature as a sign of substructure led to the conclusion that up to 70% of the X-ray clusters were structured. If their results are reinterpreted on the light of the conclusions of this work, we find that the above fraction falls to less than 30%.

The hardest problem we had to deal with in this work is represented by pointing errors in X-ray images. The boresight uncertainties do not allow us to place tight constraints on any significant displacement between the peaks of the X-ray and optical emission and, even if Fig. 6 implies the positions are in agreement, any improvement will require better astrometric accuracy through new observations. Note, however, that the comparison with numerical simulations and the calculation of the parameter Γ described in Sect. 7 have been performed only using relative positions from the X-ray images and hence do not suffer of any systematic pointing error.

The new generation of X-ray telescopes (JET-X, AXAF, XMM, WFXT, ...), thanks to their higher spatial resolution and sensitivity, will presumably give us the possibility of better testing the model. Moreover, it is desirable that new observations will allow to enlarge the set of cluster observations to be compared to the predicted harmonic amplitude.

References

Abell G.O., Corwin H.G., Olwin R.P., 1989, ApJS 70 1
Allen S.W., Fabian A.C., Edge A.C., Böringer H., White D.A., 1995, MNRAS 275 741
Allen S.W., Fabian A.C., 1997, in Galactic and cluster cooling flows, Eds. N. Soker, ASP conference series, v. 115, p. 1
Allen S.W., Fabian A.C., 1998, astro-ph/9802218
Bird C.M., 1994, AJ 107 1637
Davis D.S., 1994, Ph.D. Thesis, LHEA, GSFC
Fabian A.C., 1994, ARA&A 32 227
Friaca A.C.S., 1993, A&A 269 145
Grebenev S.A., Forman W., Jones C., Murray S., 1995, ApJ 445 607
Hill J.M., Hintzen P., Oegerle W.R. et al., 1988, ApJ 332 L23
Huang Z., Sarazin C.L., 1998, ApJ 496 728
Lazzati D., Campana S., Rosati P., Chincarini G., Giacconi R., 1998 A&A 331 41
Malumuth E.M., 1992, ApJ 386 420
Malumuth E.M., Richstone D., 1984, ApJ 276 413
Malumuth E.M., Kriss G.A., Dixon W.V.D., Ferguson H.C., Ritchie C., 1992, AJ 104 495
Meiksin A., 1988, ApJ 334 59
Mohr J.J., Fabricant D.G., Geller M.J., 1993, ApJ 413 492
Mohr J.J., Evrard A.E., Fabricant D.G., Geller M.J., 1995, ApJ 447 8
Nakamura F.E., Hattori M., Mineshige S., 1995, A&A 302 649
Oegerle W.R., Hill J.M., 1992, AJ 104 2078
Oegerle W.R., Hill J.M., 1994, AJ 107 857
Pierre M., Starck J.L., 1998, A&A 330 801
Richstone D., Malumuth E.M., 1983, ApJ 268 30
Richstone D., Loeb A., Turner E.L., 1992, ApJ 393 477

Rosati P., 1995, Ph.D. Thesis, Rome University

Sarazin C.L., 1988, X-ray emission from clusters of galaxies, Cambridge University Press

Sarazin C.L., McNamara B.R., 1997, ApJ 480 203

Sharples R., Ellis R., Gray P., 1988, MNRAS 231 479

Snowden S.L., 1995, Cookbook for analysis procedures for ROSAT XRT/PSPC observations of extended sources and the diffuse background, LHEA, GSFC

Snowden S.L., Mc Cammon D., Burrows D.N., Mendenhall J.A., 1994, ApJ 424 714

White D.A., Jones C., Forman W., 1997, MNRAS 292 419

Zabludoff A.I., Huchra J.P., Geller M.J., 1990, ApJS 74 1

Zimmermann H.U., 1994, IAU Circ. 6102